Theoretical Investigations of the Effects of J-Aggregation on the Linear and Nonlinear Optical Properties of *E*-4-(4-Dimethylaminostyryl)-1-methylpyridinium [DAMS$^+$]

Francesca Nunzi, Simona Fantacci,* Filippo De Angelis, and Antonio Sgamellotti

Istituto CNR di Scienze e Tecnologie Molecolari (ISTM-CNR), c/o Dipartimento di Chimica, Università degli Studi di Perugia, via Elce di Sotto 8, I-06123 Perugia, Italy

Elena Cariati and Renato Ugo

Dipartimento di Chimica Inorganica, Metallorganica e Analitica dell'Università degli Studi di Milano and UdR dell'INSTM di Milano, via Venezian 21, 20133 Milano, Italy

Piero Macchi

Dipartimento di Chimica Strutturale e Stereochimica Inorganica and Centro di Eccellenza CIMAINA dell'Università degli Studi di Milano, via Venezian 21, 20133 Milano, Italy

Received: May 15, 2007; In Final Form: October 26, 2007

J-type aggregation of organic chromophores into inorganic host matrixes provides a useful route toward materials showing strong second-order nonlinear optical (NLO) response. The increased NLO response of J-aggregates is related to the peculiar arrangement of the NLO-phores into the host matrix, which produces the appearance of a narrow and intense band in the material electronic absorption spectrum, red-shifted with respect to the main absorption band of the isolated NLO-phore. A theoretical investigation, based on DFT, TDDFT, and ZINDO calculations on the relationship between the structural features of various [DAMS$^+$] ([DAMS$^+$] = *E*-4-(4-dimethylaminostyryl)-1-methylpyridinium) dimeric or oligomeric aggregates and their linear and nonlinear optical properties shows that the appearance of a new red-shifted absorption band, typical of J-aggregation, is associated with interchromophoric transitions of charge-transfer character, due to the splitting of HOMO and LUMO levels. The intensity of this latter band increases by increasing the number of NLO-phores in a model of oligomeric arrangement of J-aggregates. The calculated quadratic hyperpolarizabilities for the mostly responsive J-type trimeric aggregates of [DAMS$^+$] are found to largely exceed that of three isolated NLO-phores, confirming a cooperative NLO strong contribution due to J-aggregation. Finally, our DFT and TDDFT calculations on eclipsed or with opposite dipole dimeric H-aggregates of [DAMS$^+$] show a splitting of HOMO and LUMO levels, which gives place to interchromophoric transitions of charge-transfer character but blue-shifted, as observed experimentally.

1. Introduction

In the last few years, the design of new and more efficient materials for nonlinear optics (NLO) has interested many areas of chemistry, physics, and material science because of their potential applications for telecommunications, optical computing, and optical data storage.[1,2] The various electronic factors that favor large quadratic hyperpolarizabilities of organic and organometallic molecular NLO-phores are now well-known.[1,2] For crystalline materials, the noncentrosymmetric arrangement of the molecular NLO-phores represents the necessary prerequisite for a second-order NLO response.[1,2] The achievement of a noncentrosymmetric packing is not trivial because a large molecular dipole of the NLO-phore, which usually favors a high second-order NLO response, is a potential driving force toward a centric crystalline assembling.

Various strategies have been followed to obtain noncentrosymmetric arrangements (or to artificially induce a noncentrosymmetric packing). Electrical poling of the NLO-phores dispersed in a polymeric matrix may provide significant macroscopic second-order susceptibility ($\chi^{(2)}$) of the resulting composite polymeric materials because of the electrical isoorientation of the NLO-phores, which, however, shows a poor long-term stability.[3,4] An alternative approach, originally proposed by Meredith,[2] consists of the exploitation of the Coulombic interactions of ionic NLO-phores with specific counterions that could overwhelm the centro-symmetrical dipole−dipole interactions, allowing a possible acentric assembly of the crystalline network. Marder largely applied the "salt approach" to cationic stilbazolium-type NLO-phores characterized by large quadratic hyperpolarizabilities to produce acentric crystalline materials with high SHG (second harmonic generation) by controlling the nature of the counterion. Within these salts, *E*-4-(4-dimethylaminostyril)-1-methylpyridinium *para*-toluenesulfonate, [DAMS$^+$][PTS$^-$], has been identified as a crystalline material with very high SHG.[5]

A different approach to solve the problem of acentric crystal packing was followed by the insertion, by ion exchange, of the [DAMS$^+$] NLO-phore into a layered inorganic anionic host lattice, (MPS_3, with M = Mn^{2+} and Cd^{2+}) to produce hybrid inorganic−organic materials with strong SHG.[6] In these materials, the [DAMS$^+$] NLO-phores, upon intercalation into the centrosymmetric layered MPS_3 lattice, spontaneously adopt a

* Corresponding author. E-mail: simona@thch.unipg.it.

10.1021/jp073748d CCC: $40.75
Published on Web 01/04/2008

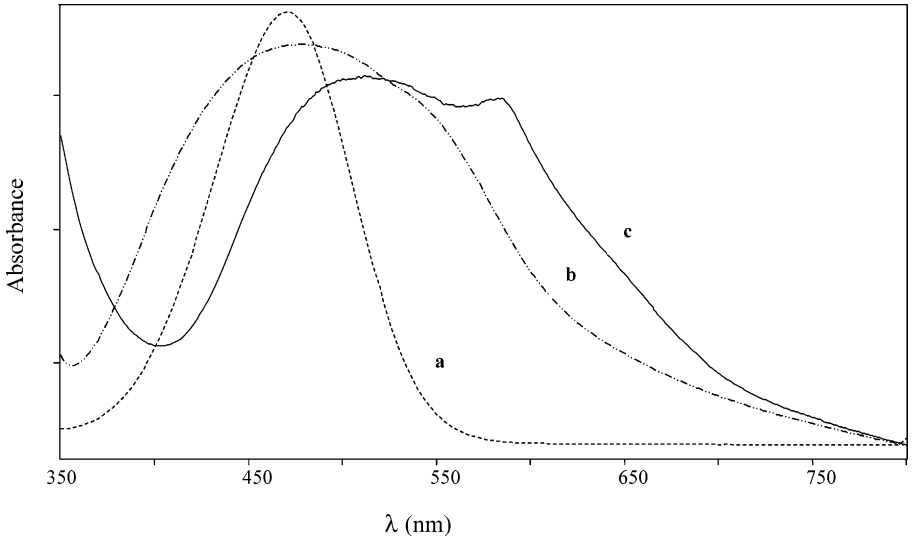

Figure 1. Absorption electronic spectra of (a) [DAMS$^+$]I in CH_3CN solution; (b) [DAMS$^+$]I in KBr pellets; (c) [DAMS$^+$][Cu_5I_6] in KBr pellets.[15]

noncentrosymmetric arrangement through the formation of J-type (or Scheibe)[7] aggregates. The intercalated J-aggregates of [DAMS$^+$] show a characteristic narrow band in the visible region of the absorption spectrum red-shifted with respect to the absorption band typical of monomeric [DAMS$^+$] in solution. This feature is typical of J-type aggregation, as opposed to H-aggregation of chromophores that shows an absorption band blue-shifted with respect to that of the monomeric chromophore.[8] Other examples of hybrid inorganic−organic salts characterized by strong second-order NLO response have been reported, where [DAMS$^+$] or related stilbazolium type NLO-phores are orderly intercalated, often as J-aggregates, within various host inorganic lattices.[9−15] For instance, recently we reported on the new layered salt [DAMS$^+$][Cu_5I_6] showing very strong SHG. The host anionic inorganic lattice consists of CuI slabs stacked along the trigonal axis while the [DAMS$^+$] cations arrange as J-type aggregates layered between the CuI slabs as supported by the presence of the typical red-shifted narrow absorption peak at 580 nm, indicative of J-aggregation (Figure 1). Unfortunately, because single crystals of [DAMS$^+$][Cu_5I_6] could not be obtained, a structural characterization of the packing geometries of the J-aggregates of the [DAMS$^+$] NLO-phore was not achieved.[15]

Despite the large interest on the role of J-aggregation as origin of the strong second-order NLO response of this kind of hybrid materials, only a few theoretical works, based on semiempirical methods, have been reported to date on aggregates of organic[16−20] or organometallic chromophores.[16c,20−23] In this paper, we report a full quantum mechanical investigation on the electronic and optical properties of [DAMS$^+$] J-aggregates by means of DFT, TDDFT, and ZINDO calculations, with the aim to find the electronic origin of the typical linear and nonlinear optical properties of these J-aggregates. In particular, in Section 3.1 we investigated the isolated [DAMS$^+$] NLO-phore both in vacuo and in solution, also taking into account the effect of the counterion on the optical properties. We find an excellent agreement between the experimental spectrum and those computed at different levels of theory. Moreover, we assign the absorption band at 471 nm as a charge-transfer transition from the $N(Me)_2$ donor group of the chromophore to the methylpyridinium acceptor moiety. In Section 3.2 we analyzed several dimeric arrangements of [DAMS$^+$] demonstrating that the slipped conformation shows spectroscopic features and an increased second-order NLO response both consistent with a J-aggregation. Notably, we assign the absorption band, characteristic of the J-aggregation, as a charge transfer interchromophoric transition. Finally, in Section 3.3 we take into consideration clusters of increasing size using ZINDO calculations, pointing out that the lower energy band, characteristic of J-aggregation, gains intensity upon increasing the number of NLO-phores and that a cooperative effect in the hyperpolarizability is present.

2. Method and Computational Details

The analytical calculation of the quadratic hyperpolarizability tensor can be performed in two different but equivalent approaches,[24] that is, the coupled perturbed and the time dependent, both applicable within DFT.[25,26] Quadratic hyperpolarizabilities can be also computed by numerically evaluating the necessary derivatives in the presence of an external electric field; these are called finite fields (FF) methods. A different approach is that based on the sum over states (SOS) method, which leads to quadratic hyperpolarizabilities by determination of all of the excitation energies and transition dipole moments between all couples of states and ground- and excited-state dipole moments.[27,28] This approach requires, therefore, the calculation of dipole matrix elements between all possible couples of excited states (three level terms), in addition to the ground to excited states transition dipole moments (two level terms). It turns out, however, that two- and three-level terms show approximately the same scaling with the number of excited states as two-level terms so that the latter can be used for a semiquantitative assessment of the contributions to the quadratic hyperpolarizability.[16c]

A well-known oversimplification of the SOS approach is the two-level model approximation,[28] which takes into account only one more relevant charge-transfer excited state along the dipole axis (the *z* axis), leading to the following expression for the static quadratic hyperpolarizability:

$$\beta_{zzz}^{0} \propto r^2 \Delta\mu_{eg}/\nu_a^2$$

where r is the transition dipole moment, $\Delta\mu_{eg}$ is the difference between ground- and excited-state dipole moments, and ν_a is the frequency of the electronic transition.

Because there is a direct relation between the excited states and the second-order NLO response of a NLO-phore, as

indicated by the SOS approach and simplified in the two-level approximation described above, we necessarily have to investigate as a first step an accurate theoretical reproduction of its optical absorption spectrum. In this respect, methods based on a Hartree−Fock representation of the ground state seem to be of little quantitative value to support further calculations of second-order NLO properties, due to the fact that both configuration interaction with single excitations (CIS) and time-dependent Hartree−Fock (known also as RPA) methods usually lead to a large overestimation of the excitation energies. DFT methods, however, offer a powerful ground-state tool, and time-dependent DFT (TDDFT) has proven to provide excitation energies to a high degree of accuracy also for very complex systems composed by several hundred atoms including transition metals.[29] Therefore, coupled perturbed Kohn Sham (CPKS) and TDDFT methods might, in principle, represent good candidates for the calculation of second-order NLO properties, even though some inaccuracies of these methods to compute NLO have been reported.[24] It has been reported, moreover, that TDDFT methods using conventional exchange-correlation functionals can fail in calculating charge-transfer intramolecular transitions and excitations in spatially separated systems.[30−32]

A combined FF and CPKS formalism to calculate static quadratic hyperpolarizabilities is implemented in the Gaussian03 package (G03),[33] in which numerical differentiation of analytic polarizabilities in the presence of an external electric field is performed. A TDDFT approach to static and frequency-dependent quadratic hyperpolarizabilities is implemented, however, in the ADF package.[26b,34,35] The TDDFT approach to calculate second-order NLO properties is in principle more efficient than the FF-CPKS one because in the latter seven polarizability calculations need to be performed for asymmetric systems (one reference calculation in the absence of the field and six calculations in the presence of different directions of the electric field), while in TDDFT a single response calculation yields the entire frequency-dependent hyperpolarizability tensor. On the basis of the above critical analysis of the theoretical tools available to calculate both ground and excited states and therefore second-order NLO properties of a NLO-phore, both TDDFT and FF-CPKS calculations have been performed here. Indeed, the high computational efficiency of the linear-response TDDFT implementation of the ADF program was first exploited to perform an assessment of the level of theory and to provide a preliminary screening of the absorption and second-order NLO properties of [DAMS$^+$] as a monomer or as various dimeric aggregates. Subsequently, we employed the G03 program package to evaluate the effect of hybrid exchange-correlation functionals, that is, containing some amount of Hartree−Fock exchange, on the linear optical and second-order NLO properties. To calculate the absorption and the second-order NLO response of a specific kind of large [DAMS$^+$] aggregate, we finally resort to the semiempirical ZINDO approach.[36] This choice is necessarily dictated by the large dimensions of the investigated system (exceeding 370 atoms) and by the large number (up to 100) of excited states that need to be computed.

The molecular geometry of the monomer [DAMS$^+$] was first optimized by DFT calculations under C_s symmetry constraints. Such an optimized geometry was then used to construct the various dimeric arrangements. The electronic excitation energies and quadratic hyperpolarizabilities were calculated by means of the TDDFT approach for both the monomeric [DAMS$^+$] and various dimers. In particular, we calculated both the static and the frequency-dependent quadratic hyperpolarizabilities using an incident wavelength of 1907 nm, corresponding to the incident laser frequency used to obtain many experimental data.[15] The 10 lowest spin-allowed singlet−singlet transitions were thus calculated, employing a standard double-ζ basis set including polarization functions (DZP), consisting of Slater-type orbitals (STOs), with the cores (1s for C and N) kept frozen. For the geometry optimization of the monomer and in the ground-state SCF step of the TDDFT calculations, we used the BP86 gradient-corrected exchange-correlation (XC) functional[37,38] (including the Vosko−Wilk−Nusair LDA parametrization).[39] In the post-SCF step of the TDDFT calculations, we used the adiabatic XC kernel based on the local density approximation (ALDA). To check the convergence of the calculated properties with the basis set expansion, we also carried out geometry optimizations and TDDFT calculations for the monomer and for a representative dimer using a larger basis set of uncontracted triple-ζ STOs plus polarization functions (TZP). Test calculations have also been performed on monomeric [DAMS$^+$] and on a representative dimer by employing the asymptotically correct van Leeuwen−Baerends XC functional (LB94)[40] to evaluate the dependence of our TDDFT excitation energies and quadratic hyperpolarizabilities on the choice of the XC functional. For G03 calculations, we used the B3LYP XC functional[41] together with a 6-31G(d,p) polarized split valence basis set.[42] For monomeric [DAMS$^+$], we also investigated the effect of solvation on calculated TDDFT excitation energies, by means of the nonequilibrium C−PCM version,[43] as implemented in the G03 program. To compare the calculated absorption spectrum of [DAMS$^+$] with the experimental one, transition energies and oscillator strengths have been convoluted by Gaussian functions with a σ of 0.2 eV. The calculated quadratic hyperpolarizability vector components ($\beta_{vec} = \Sigma_i \mu_i \beta_i / (\Sigma_i \mu_i^2)^{1/2}$, $\beta_i = \beta_{iii} + {}^1/_3 \Sigma_{i \neq j} \beta_{ijj} + \beta_{jij} + \beta_{jji}$) have been reported according to the "phenomenological" convention.[44] Frequency-dependent quadratic hyperpolarizabilities (β_{SHG}) have been calculated, as reported above, considering an incident laser wavelength of 1907 nm. For G03 calculations, excited-state dipole moments have been calculated using the rhoCI density.[45] Finally, we calculated the static quadratic hyperpolarizability by means of the SOS-ZINDO method, using 40 HOMOs and 40 LUMOs for the monomer, the dimer, and the trimer. These calculations have been performed with the Hyperchem package.[46]

3. Results and Discussion

3.1. Theoretical Investigation of Linear and Nonlinear Optical Properties of [DAMS$^+$] as a Monomer. We first investigated the geometrical and electronic properties of the [DAMS$^+$] NLO-phore as a monomer by performing DFT and TDDFT calculations employing various density functionals and basis sets in order to verify the accuracy of the computational approach. In fact, the computed molecular geometries, electronic transitions, and quadratic hyperpolarizability have been compared with the available experimental data in order to calibrate the computational setup. In Table 1, the molecular geometry of [DAMS$^+$] optimized at different levels of theory is reported together with the X-ray structure of [DAMS$^+$].[47] The geometrical parameters have been optimized with ADF code, using the BP86 XC functional and DZP and TZP basis sets, and with G03, using the B3LYP functional and a 6-31G(d,p) basis set. No differences have been computed using DZP and TZP basis sets, while differences within 0.01 Å and fractions of degree have been computed with G03 at the B3LYP/6-31g(d,p) level. The optimized geometries are in reasonable agreement with the

TABLE 1: DFT Optimized Main Geometrical Parameters for the [DAMS$^+$] Molecule[a]

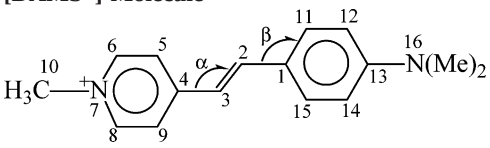

	BP86/DZP	BP86/TZP	B3LYP/6-31G(d,p)	exp[47]
R1−2	1.418	1.419	1.427	1.452(7)
R2−3	1.374	1.374	1.375	1.32(3)
R3−4	1.415	1.417	1.425	1.451(13)
R4−5	1.424	1.424	1.427	1.393(16)
R5−6	1.365	1.366	1.369	1.37(2)
R6−7	1.366	1.366	1.364	1.36(2)
R7−8	1.363	1.363	1.366	1.35(3)
R7−10	1.470	1.470	1.472	1.46(2)
R8−9	1.367	1.367	1.368	1.37(2)
R9−4	1.421	1.422	1.427	1.400(14)
R1−11	1.415	1.416	1.419	1.396(10)
R11−12	1.373	1.374	1.377	1.382(16)
R12−13	1.425	1.426	1.425	1.401(12)
R13−14	1.429	1.429	1.429	1.396(14)
R14−15	1.370	1.371	1.375	1.373(14)
R15−1	1.418	1.417	1.420	1.394(12)
R13−16	1.359	1.359	1.369	1.38(2)
R16−Me	1.458	1.459	1.461	1.45(2)
α	125.8	125.9	125.4	126(3)
β	120.1	119.9	119.2	120(3)

[a] Bond lengths in angstroms and bond angles in degrees. Experimental values are averages among the distances obtained by single-crystal X-ray diffraction on several salts containing [DAMS$^+$] cation (standard deviations are reported in parentheses).

TABLE 2: TDDFT Computed Ground States Dipole Moments (D), Excitation Energy (eV), and Oscillator Strength (*f*) Involving the Lowest Singlet Excited State S_1, Static and SHG β_{vec} Values (10^{-30} esu^{-1} cm^5) Computed at Different Levels of Theory[a]

	BP86/ DZP	BP86/ TZP	LB94/ DZP	LB94/ TZP	B3LYP/ 6-31g(d,p)
μ	5.0	5.0	4.9	4.9	6.2
E (S_0-S_1)	2.501	2.496	2.428	2.395	2.696
f (S_0-S_1)	1.144	1.122	1.111	1.078	1.376
β_{vec}	17.0	17.1	17.6	17.8	35.0
β_{vec} (SHG)	23.6	23.9	24.9	25.5	

[a] All of the calculations have been performed with the same molecular orientation and framework origin, the latter being located in correspondence to C_2.

available X-ray data obtained for several salts containing the [DAMS$^+$] cation.[47] All stilbene-like molecules, also [DAMS$^+$], in the solid state, are subject to the dynamic disorder produced by the so-called "pedal motion"[48] around the central carbon−carbon double bond, which usually results in an apparently shorter C−C double bond distance. Our DFT calculations (see Table 1), indeed, provide a C_2-C_3 distance of 1.374−1.375 Å, quite longer compared with the average experimental value of 1.32(3) Å.[47]

Results of TDDFT excited-state calculations obtained in vacuo with different functionals and basis sets are reported in Table 2. For the sake of comparison, here we discuss data related to the BP86/DZP optimized geometry. At all levels of theory, the lowest singlet excited state (S_1) is calculated to be an intense single transition essentially involving the HOMO and LUMO levels, see Figure 2. Both HOMO and LUMO orbitals are delocalized over the entire molecule, but the HOMO is more localized on the $N(Me)_2$ donor group and on the structurally connected aromatic ring, while the LUMO is more localized on the methylpyridinium acceptor moiety. This electronic system is a prototypical push−pull NLO-phore, characterized by an intense transition with partial intramolecular charge-transfer character. All of the other transitions within 0.5 eV have much lower oscillator strengths so that the transition involving S_1 can be unambiguously assigned to the experimental absorption maximum at 471 nm (2.6 eV).[15] For the investigated GGA functionals, the increase of the basis-set quality from DZP to TZP does not lead to appreciable changes of the energy and strength of the transition involving S_1, and thus of the calculated absorption spectrum. Compared to the BP86 functional, the asymptotically correct LB94 functional delivers only a slightly red-shifted and lower intensity transition for the first excited state, S_1 (see Table 2). The same trend has been observed for calculated dipole moments and quadratic hyperpolarizabilities, which, within the GGA functionals considered here, are almost identical and independent from the choice of the basis set (see Table 2). Moving to the B3LYP/6-31g(d,p) level of theory, the S_1 excited state is calculated at a slightly higher energy compared to the energy calculated with the GGA approach, with an increased intensity of the transition involving S_1. The higher transition energy calculated with B3LYP can be directly related to the increased HOMO−LUMO gap calculated using this functional. In addition, while the GGA calculations show the presence of a second excited state just above the S_1 first excited state, B3LYP/6-31g(d,p) calculations predict a second excited state well separated in energy from the S_1 first excited state, although with a similar orbital character.

The absorption spectra of [DAMS$^+$] computed in vacuo at the BP86/DZP, LB94/DZP, and B3LYP/6-31G(p,d) levels of theory are compared to the experimental spectrum of [DAMS$^+$]I recorded in acetonitrile solution in Figure 2. The experimental absorption band at 471 nm is quite well reproduced by the computed values of 460, 496, and 511 nm obtained at the B3LYP/6-31G(p,d), BP86/DZP, and LB94/DZP levels, respectively. The difference between G03 and ADF results is not likely to be related to the different basis sets used in the two codes but rather to the different exchange-correlation functional. Inclusion of solvation effects by G03 calculations at the B3LYP/6-31g(d,p) level leads only to a slight blue-shift of the absorption band, passing from 460 nm in vacuo to 470 nm in acetonitrile.

We notice that in acetonitrile solution the salt could possibly be completely dissociated, so calculations performed on the cation should represent a good approximation; however, for sake of completeness we computed the absorption spectra of the [DAMS$^+$][PTS$^-$] system at both BP86/DZP and B3LYP/6-31G-(p,d) levels, finding the absorption maxima at 485 and 452 nm, respectively, values very similar to those discussed above for the cation, confirming that the counterion does not significantly affect the optical properties of [DAMS$^+$].

As far as the dipole moment and quadratic hyperpolarizability are concerned, qualitatively similar values are obtained using the ADF program at the various levels of theory, while a larger dipole moment and static quadratic hyperpolarizability are computed at the B3LYP/6-31g(d,p) level compared to GGA functional (Table 2), reflecting the increased charge separation associated with the Hartree−Fock exchange contribution to the overall exchange-correlation functional. Moreover, the values of the frequency-dependent quadratic hyperpolarizability are about 40% larger than the corresponding static values. The value of quadratic hyperpolarizability determined experimentally by the EFISH technique considering an incident laser wavelength of 1907 nm for [DAMS$^+$]I in $CHCl_3$ solution ($c = 5 \times 10^{-4}$ M) is around 69.4×10^{-30} esu^{-1} cm^5,[49] which is in reasonable agreement with our calculated values in vacuo, especially

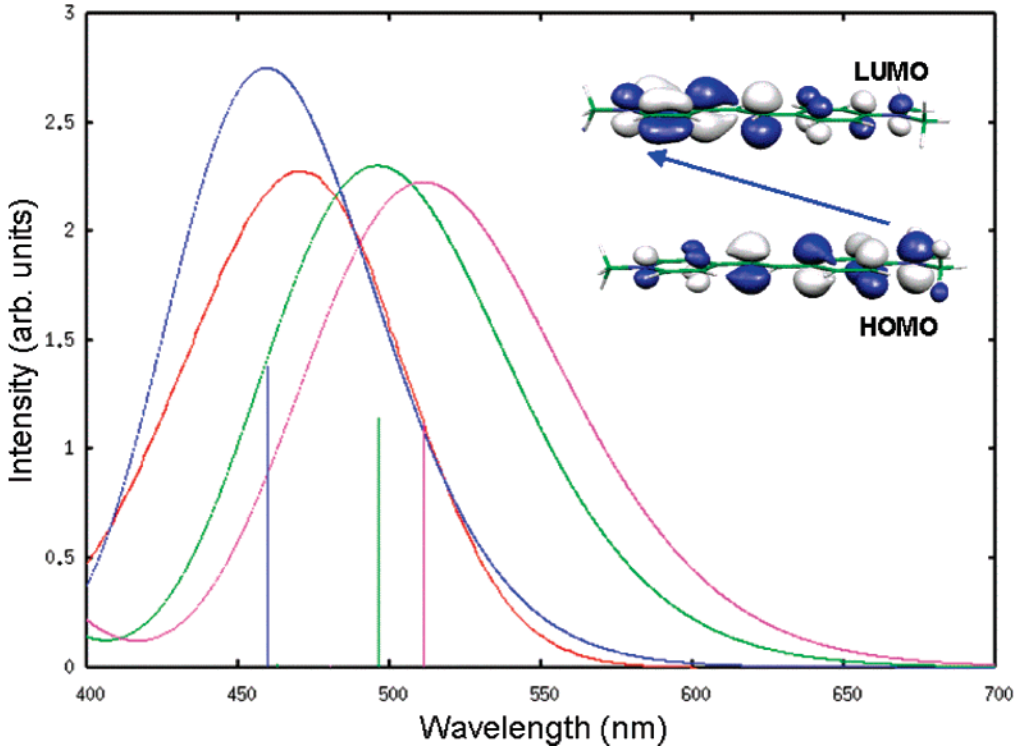

Figure 2. Comparison between the experimental (red line) and theoretical spectra of [DAMS$^+$] computed in vacuo at the BP86/DZP (green line), LB94/DZP (magenta line), and B3LYP/ 6-31G(p,d) (blue line) levels of theory.

considering that the experimental measurements refer to a [DAMS$^+$] cation coupled with an anionic counterion and the neglect of dispersion effects for B3LYP results. In particular, the frequency-dependent quadratic hyperpolarizability computed at different levels of theory with ADF provides values ranging from 23.6 to 25.5 $\times$ 10^{-30} esu^{-1} cm^5, while the static hyperpolarizability was found to be 35.0 $\times$ 10^{-30} esu^{-1} cm^5 at the B3LYP /6-31g(d,p) level, see Table 2. To evaluate the counterion effect on the NLO optical response, we computed β_{vec} for the experimentally characterized [DAMS$^+$][PTS$^-$] system at the BP86/DZP and B3LYP/6-31g(d,p) levels, consistently obtaining ca. 1.4 larger values than those computed for the [DAMS$^+$] cation.

On the basis of efficiency grounds and on the above results, we have thus selected the BP86/DZP level of theory and the ADF program to explore the relation between the geometrical arrangement and the absorption and second-order NLO properties of several dimeric arrangements of the NLO-phore [DAMS$^+$]. Indeed, LB94 and BP86 were found to give essentially the same results, but the former allows us to speed-up the calculations due to the use of an efficient fitting procedure of the Hartree potential in the SCF step. Consequently, we repeated calculations at the B3LYP/6-31g(d,p) level with the G03 program only for some selected configurations of dimeric aggregates.

3.2. Theoretical Investigation of Linear and Nonlinear Optical Properties of [DAMS$^+$] as Various Dimeric Aggregates. In all of the dimeric structures investigated, we retained the molecular geometry of monomeric [DAMS$^+$], optimized at the BP86/DZP level, but taking into consideration several interchromophoric relative orientations. In particular, we studied the six different geometrical dimeric arrangements shown in Scheme 1. The coordinate system was chosen so that the largest dipole moment component is parallel to the *x* axis. We first studied the two monomers in a cofacial eclipsed conformation (A). Slipped conformations have been thus investigated by parallel translations of conformation A along the *x* axis (B_x) and *y* axis (B_y), and along the *x* axis fixing a d_y in order to reach the overlap of the phenyl and pyridinium rings (B_{xy}), while a staggered conformation (C) was generated by rotation (α) of one chromophore in the *xy* plane. The final sixth conformation (D) was gathered by flipping one chromophore about the longitudinal molecular axis, the *x* axis in this case. For the cofacial eclipsed conformation A, we initially analyzed an interchromophoric distance d_z ranging between 2.5 and 10.0 Å. As reported by other authors already,[31,32] however, for large interchromophoric separations (>4.0 Å) TDDFT calculations yield two essentially degenerate excitation energies corresponding to the difference between the KS eigenvalues rather than the correct TDDFT excitation energy (see Supporting Information). We therefore limited our discussion of TDDFT results to regions of significant overlap between the two interacting [DAMS$^+$] NLO-phores, thus finally choosing an interplanar distance d_z of 3.5 Å (see below). For B_x conformations, the slippage distances along the *x* axis were varied between -10 and $+10$ Å. For B_y conformations, the slippage distance along the *y* axis was varied between 0.0 and 5.0 Å. In the case of B_{xy} conformations, we applied, to an initial conformation with overlap of phenyl and pyridinium rings of the two NLO-phores ($d_x = -6.6$ Å and $d_y = 1.2$ Å), a slippage distance varied along the *x* axis with step of $d_x = \pm 0.4$ Å up to $d_x = -9.0$ Å and $d_x = -5.0$ Å, maintaining fixed $d_y = 1.2$ Å. For the staggered C conformation, we varied the rotation angle α from 0° to 180° (the latter arrangement corresponding to A conformation but "head-to-tail" one). For the flipped D conformation, the rotation angle α was varied from 0° to 45°, while to evaluate the effect of larger rotations, with α ranging from 0° to 180°, we considered a d_z interchromophoric distance of 7.0 Å, see the Supporting Information.

By decreasing the interplanar distance d_z of the cofacial conformation A below 3.5 Å, the total energy continues to increase not showing a minimum. We noticed that going from 10.0 to 3.5 Å the energy increases by only 25.2 kcal/mol, while

SCHEME 1

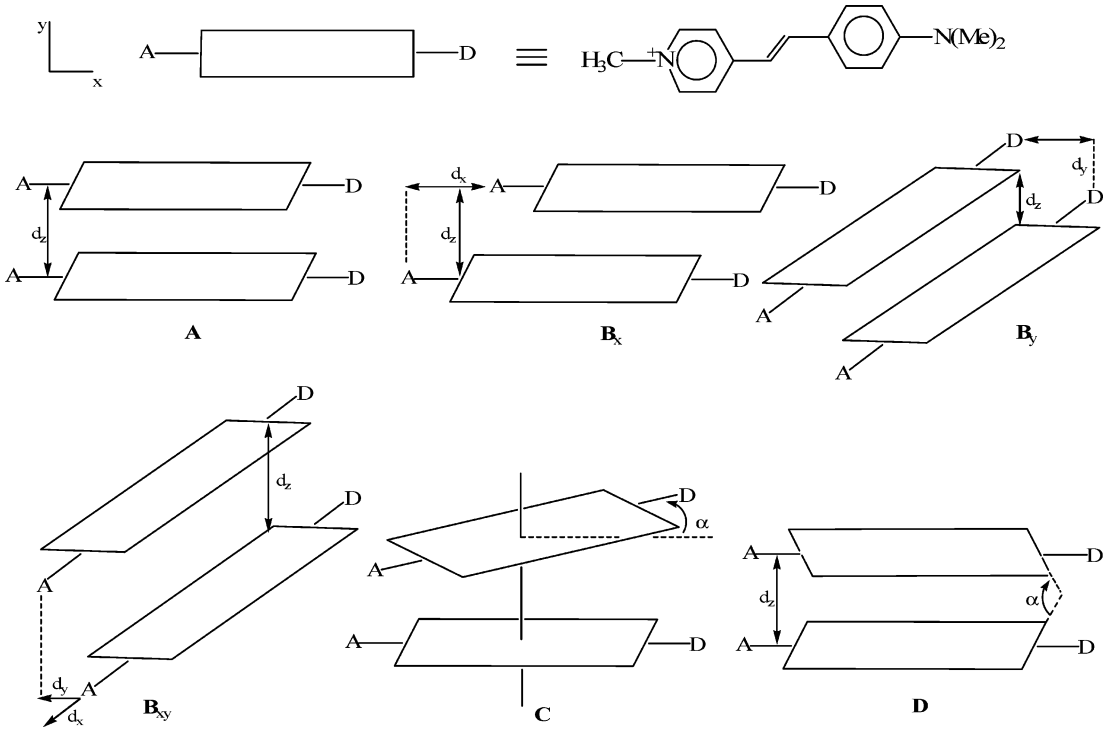

going from 3.5 to 2.5 Å the energy increases as much as 373.1 kcal/mol, essentially dominated by the strong electrostatic repulsion between the two positively charged NLO-phores with an overlap between the monomer wavefunctions. For neutral related stylbazolic NLO-phore in a cofacial conformation A with d_z ranging from 4.0 to 2.5 Å, the total energy shows a minimum for $d_z = 3.5$ Å, while going from 3.5 to 2.5 Å the energy increases but only by 199.3 kcal/mol. The presence of a minimum and the reduced increase of energy by decreasing from 3.5 to 2.5 Å show that the interchromophoric distance is clearly related to the lack of strong electrostatic repulsion between the two neutral NLO-phores, as opposed to two cationic [DAMS$^+$] moieties. When considering the B_x conformation, by reducing the interchromophoric distance d_z for a fixed slippage distance d_x of 5.0 Å, a minimum of the total energy is found for $d_z = 4.0$ Å. By further reducing d_z below 3.0 Å, a sharp energy increase takes place, as for the cofacial conformation A. The above results suggest that, even including the effect of the inorganic lattice with compensating negative charges, it is very difficult for dimeric aggregates of the NLO-phore [DAMS$^+$] to reach interchromophoric distances below 3.0 Å. Moreover, we also investigated a neutral [DAMS$^+$][PTS$^-$] dimer, finding an energy increase of only 18.3 kcal/mol from an infinite separation to a slipped B_x configuration with $d_z = 3.5$ Å and a slippage distance d_x of 5.0 Å, to be compared to an energy increase of 32.4 kcal/mol for the same configuration without the [PTS$^-$] counterion. As expected, inclusion of a negative counterion saturating the positive chromophore charge reduces the electrostatic repulsion drastically between the two monomers in the considered dimeric arrangement.

On the basis of these results, we have always investigated in detail conformations A, B_x, B_y, B_{xy}, and C with $d_z = 3.5$ Å and only briefly those with $d_z = 3.0$ Å for comparison. The orbital energy diagram for the dimeric aggregates as a function of the interchromophoric distance d_z for the cofacial A conformation or of the slippage distance, d_x, for a fixed value of d_z of 3.5 Å, is reported in Figure 3. As the interchromophoric distance is decreased, the two sets of occupied and unoccupied molecular orbitals begin to interact and their energies split according to the so-called eccitonic model.[17] However, the two HOMO and LUMO orbitals remain essentially localized on each monomer with little mixing within the two sets. Interestingly, while for the cofacial A conformation the orbital splitting increases, as expected, by decreasing the interplanar distance d_z, for the slipped B_x arrangements, taking d_z constant, the HOMOs splitting keeps on increasing with increasing slippage, suggesting that the reciprocal electronic perturbation between the two NLO-phores increases as a "head-to-tail" arrangement is approached, in line with previous observations by Di Bella et al.[16a]

On moving to the discussion of TDDFT results, in Table 3 we have summarized the most relevant transitions of characteristic dimeric configurations. We labeled these computed transitions as I, II, and III for increasing energies, with transition III being related to the main absorption band of the monomer. The totality of computed transitions related to all of the investigated dimeric conformations were reported in the Supporting Information. For the cofacial dimeric conformation A with interchromophoric distances $\leq$4.0 Å, two transitions are calculated increasingly blue-shifted with respect to that computed for the isolated [DAMS$^+$] NLO-phore as the interchromophoric distance is reduced, and the sum of their oscillator strengths is slightly lower than that calculated for two isolated chromophores (1.70−1.86 with respect to 2.29, see Table 2). Because the appearance of a new band at higher energy with respect to that of the isolated NLO-phore is the typical spectroscopic signature of H-aggregates,[8] as the eclipsed cofacial dimeric conformation with monomeric dipoles aligned in a parallel arrangement, we can assign the origin of this new absorption to the splitting of HOMO and LUMO levels due to the reciprocal perturbation. No transitions of relevant intensity are calculated below these main transitions for the eclipsed cofacial dimer A, as expected because the interchromophoric excitations are symmetry forbidden in the cofacial conformation.[17]

For the slipped conformation B_x, taking into consideration d_z interchromophoric distances of 3.0 and 3.5 Å, by increasing

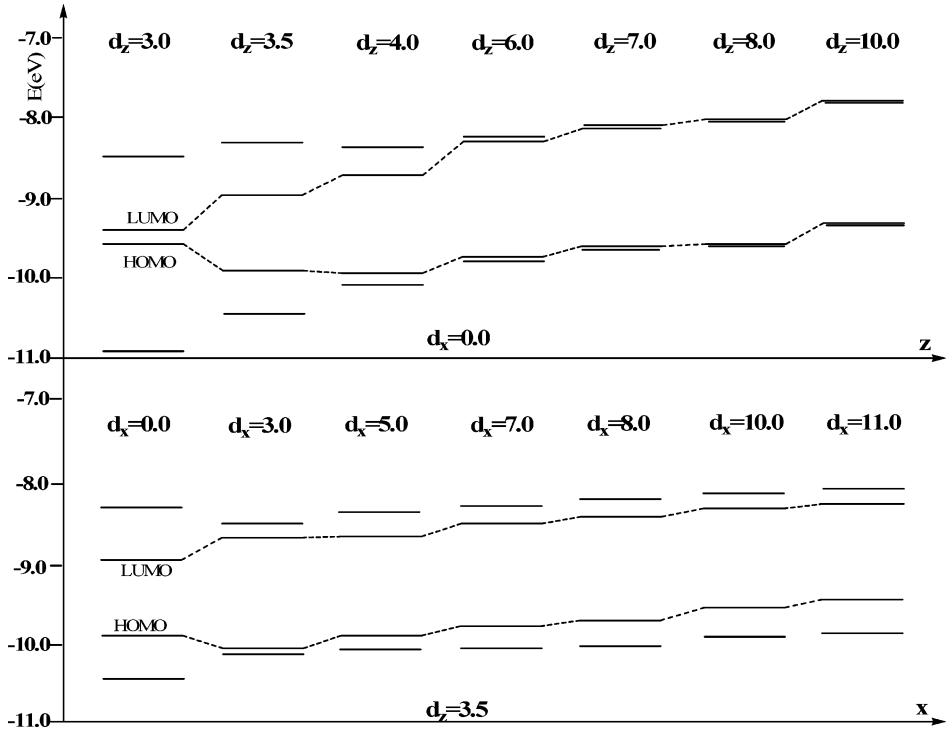

Figure 3. Schematic representation of the orbital energies (eV) for the eclipsed cofacial (A) and slipped (B_x) dimeric arrangements. Only the HOMO−1/HOMO and LUMO/LUMO+1 are reported for clarity.

TABLE 3: Excitation Energy (eV), Oscillator Strength (f), and Composition of the Most Significant Singlet Excited States for Selected Dimeric Conformations Computed at the BP86/DZP and B3LYP/6-31G(d,p) Levels of Theory[50]

Trans.	E	f	MOs
			A configuration $d_z = 3.5$ Å (BP86/DZP)
I	2.665	0.654	72%(H → L + 3) + 11%(H − 1 → L) + 10%(H → L + 1)
II	2.685	1.147	33%(H − 1 → L) + 32%(H → L + 1) + 21%(H → L + 3)
			B_x configuration $d_z = 3.5$ Å $d_x = 5.0$ (BP86/DZP)
I	1.297	0.023	90%(H → L) + 9%(H − 1 → L)
II	1.741	0.063	75%(H − 1 → L + 1) + 23%(H → L + 1)
III	2.527	1.791	33%(H − 1 → L) + 29%(H → L + 1) + 16%(H − 1 → L + 1)
			B_x configuration $d_z = 3.5$ Å $d_x = 5.0$ (B3LYP/6-31g(d,p))[50]
I	1.877	0.037	92%(H → L) + 7%(H - 1 → L)
II	2.178	0.123	72%(H − 1 → L + 1) + 24%(H → L + 1)
III	2.772	2.476	32%(H − 1 → L) + 18%(H → L + 1) + 14%(H − 1 → L + 1)
			B_{xy} configuration $d_z = 3.5$ Å $d_x = -7.4$ Å $d_y = 1.2$ Å (BP86/DZP)
I	1.213	0.034	94%(H → L)
II	1.862	0.183	78%(H − 1 → L + 1) + 11%(H − 1 → L)
III	2.456	1.264	76%(H → L + 1) + 11%(H − 1 → L + 1)
	2.492	0.812	78%(H − 1 → L) + 9%(H → L + 1)
			B_{xy} configuration $d_z = 3.5$ Å $d_x = -7.4$ Å $d_y = 1.2$ Å (B3LYP/6-31g(d,p))[50]
I	1.818	0.057	89%(H → L)
II	2.340	0.530	63%(H − 1 → L + 1) + 17%(H → L + 1) + 13%(H − 1 → L)
III	2.662	1.078	50%(H → L + 1) + 19%(H − 1 → L + 1)
			B_y configuration $d_z = 3.5$ Å $d_y = 5.0$ Å (BP86/DZP)
I	2.597	1.788	40%(H → L + 1) + 40%(H − 1 → L) + 9%(H → L + 3)
II	2.659	0.122	76%(H → L + 3) + 15%(H − 1 → L + 2)
			C configuration $d_z = 3.5$ Å $\alpha = 180^\circ$ (BP86/DZP)
I	2.583	0.913	29%(H − 1 → L) + 28%(H → L + 1) + 23%(H → L + 2) + 14%(H − 2 → L)
	2.601	0.285	74%(H → L + 2) + 8%(H − 1 → L)
II	3.057	0.728	63%(H − 2 → L) + 17%(H − 5 → L + 1) + 8%(H − 1 → L) + 8%(H → L + 1)
			D configuration $d_z = 3.5$ Å $\alpha = 30^\circ$ (BP86/DZP)
I	2.274	0.103	50%(H − 3 → L) + 22%(H − 1 → L + 1)
II	2.609	0.143	27%(H − 1 → L + 2) + 27%(H → L + 3) + 25%(H − 1 → L + 1)
	2.656	1.120	29%(H − 1 → L) + 15%(H − 1 → L + 2) + 15%(H → L + 2) + 9%(H → L + 1)
III	2.843	0.174	83%(H → L + 4)

the slippage d_x between the two chromophores, two transitions (labeled I and II) of sizable intensity are calculated at ca. 1.3 and 1.7 eV, respectively, with energies varying within approximately 0.3 eV depending on the slippage distance d_x. In all cases, at higher energy an intense transition (III) with energy similar to that of the main transition of monomeric [$DAMS^+$] is found.

In Figure 4, a plot of the excitation energies and oscillator strengths of the two low-energy transitions I and II as a function of d_x is reported. For a slippage distance of 0.0 Å, corresponding

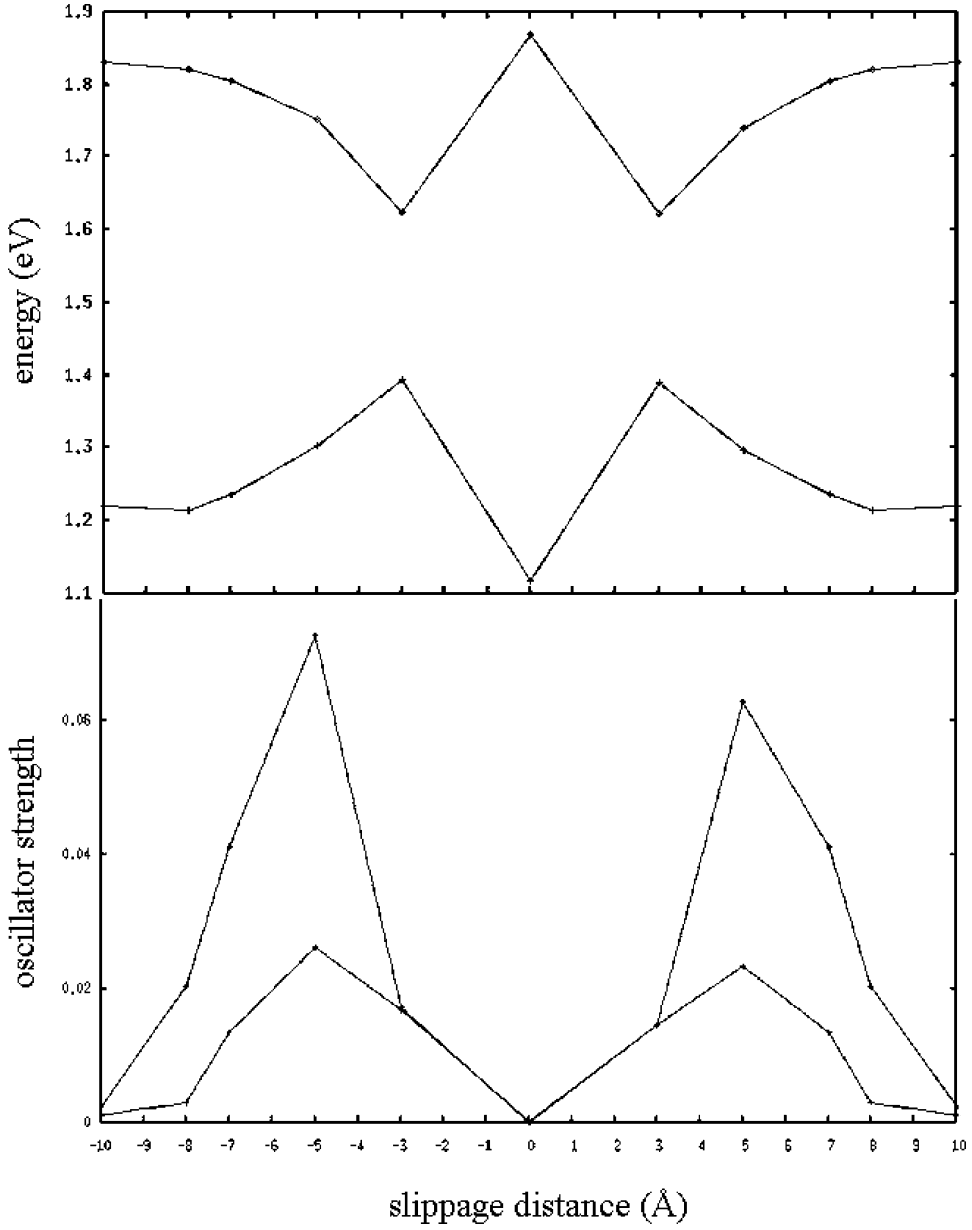

Figure 4. Excitation energies (eV) and oscillator strength as a function of the slippage distance d_x for the I (lower line) and II (upper line) transitions.

the cofacial eclipsed dimeric conformation A discussed above, the energies of the two transitions show their maximum and minimum energy values, respectively. Notably, the energies of the two transitions show complementary trends as a function of the slippage distance d_x, with mirroring increase and decrease of their energies. Large variations of the oscillator strengths are calculated along $\pm d_x$, but both transitions show a similar trend, with the lower energy transition always of lower intensity, apart for a d_x slippage of 3.0 Å, for which both transitions show almost the same oscillator strengths (see Figure 4). Maximum values of the oscillator strength are calculated for $d_x = \pm 5.0$ Å, roughly corresponding to half of the chromophore length (ca. 10.7 Å from the N head to the N tail). For such a value of d_x, the reduction of the interchromophoric distance d_z from 3.5 to 3.0 Å leads to a significant increase of the oscillator strengths of both transitions I and II, which are at similar energies (1.297 vs 1.267 and 1.741 vs 1.844 eV, respectively) but with intensities 3.42 and 5.16 times higher than those calculated for $d_z = 3.5$ Å, see Table 3 and the Supporting Information. The analysis of the TDDFT eigenvectors for a d_x slippage of ±5.0 Å, corresponding to the maximum value of the oscillator strengths, reveals that transition I involves excitation between the HOMO/LUMO (90%) and HOMO−1/LUMO (9%) orbitals, while transition II corresponds to excitations between the HOMO−1/LUMO+1 (75%) and HOMO/LUMO+1 (23%) (see Table 3 and Figure 5). Because the orbitals localized on each NLOphore are the HOMO−1 and LUMO and the HOMO and LUMO+1, respectively, we can therefore conclude that both transitions I and II have considerable interchromophoric charge-transfer characters (see Figure 5). The higher energy of transition II corresponds to a transition that involves mainly molecular orbitals more energetically spaced (HOMO−1/LUMO+1) than those involved in transition I (HOMO/LUMO). Moreover, the higher intensity of transition II is due to a sizable intrachromophoric contribution (23% HOMO/LUMO+1) responsible for the strong absorption band of the monomeric [DAMS$^+$], see Table 3. The high-energy transition III, calculated at ca. 2.53 eV, corresponds to the intrachromophoric excitation, mainly between the HOMO/LUMO+1 (29%) and HOMO−1/LUMO (33%) (see Table 3 and Figure 5).

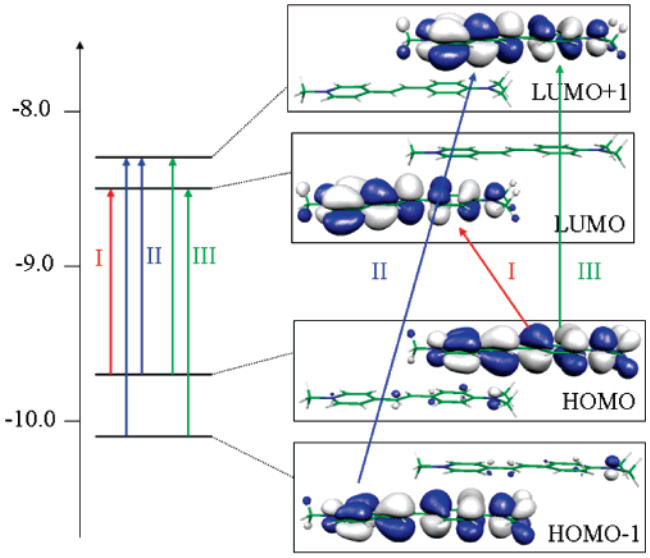

Figure 5. Schematic representation of the molecular orbitals involved in transitions I, II, and III.

From the analysis of the TDDFT eigenvalues and eigenvectors of the conformation B_{xy}, fixing d_z at 3.5 Å and d_y at 1.2 Å, and varying d_x around −6.6 Å, as discussed above, analogous to the B_x conformation, two transitions (I and II), essentially of interchromophoric character, are calculated at ca. 1.2 and 1.8 eV, respectively. Transition I is characterized by an oscillator strength smaller than that of transition II (see Table 3). Also in this case the high-energy transition III, calculated at ca. 2.5 eV, mainly corresponds to intrachromophoric excitations. The oscillator strengths of the transitions I and II show a trend similar to that typical of the d_x slippage, with maximum intensity values for both I and II transitions at $d_x = -7.4$ Å. Interestingly, the oscillator strength of transition II is higher than that calculated for the corresponding transition of the B_x conformation at $d_x = \pm 5$ Å.

In the case of the slipped conformation B_y, the analysis of the TDDFT eigenvalues varying d_y between 0.0 and 5.0 Å (for $d_y = 0.0$ Å, we still have the eclipsed cofacial conformation A) reveals that for $d_y = 1.0$ Å the main transitions are still quite similar to those computed for the cofacial conformation A in terms of both energy and oscillator strength. Only for $d_y = 2.0$ Å we calculated two almost degenerate transitions of similar intensity at 2.64 and 2.69 eV whose composition is (33% HOMO−1/LUMO+2, 22% HOMO−1/LUMO and 20% HOMO/LUMO+1) and (59% HOMO−1/LUMO+2, 20% HOMO−1/LUMO and 18% HOMO/LUMO+1), respectively (see also Supporting Information). Further moving up to $d_y < 5.0$ Å, we have one main strong transition at 2.64−2.62 eV (oscillator strength of ca. 1.7−1.8), which is essentially the sum of the single HOMO−LUMO excitations localized on the two separated NLO-phores. Only for $d_y = 5.0$ Å we computed two transitions of different intensity at around 2.6 eV slightly red-shifted with respect to those computed for smaller slippage.

The analysis of the TDDFT excitations computed for the staggered C conformation taking $d_z = 3.5$ Å and α moving from 15° to 180° initially shows trends quite similar to those of the corresponding eclipsed cofacial conformation A (see the Supporting Information): two relevant transitions are computed with one sizably more intense than the other resulting from state mixing. Only by increasing the rotation angle ($\alpha > 30°$) we calculated a new transition, at ca. 2.35−2.46 eV with a sizable oscillator strength. Moreover, for rotation angles larger than 30° all of the relevant transitions are red-shifted with respect to those computed for the eclipsed cofacial conformation A, only for the head-to-tail conformation C (with $\alpha = 180°$) we calculated slightly blue-shifted transitions of reduced intensities at 2.600 eV ($f = 0.285$), which can be associated with this new kind of H-type aggregation.

For the flipped D conformation with a rotation angle $\alpha = 15°$, we computed only one relevant transition related to the isolated chromophore HOMO−LUMO transitions, while for a rotation angle $\alpha = 30°$ the two [DAMS$^+$] units show much too short H−H distances, below 1.9 Å, resulting in interchromophore excited-state interactions (see the Supporting Information).

We can therefore conclude that, among the many conformations investigated, only the slipped conformations B_x with $d_x = \pm 5$ Å and B_{xy} with $d_x = -7.4/d_y = 1.2$ Å show transitions I and II with relevant oscillator strength red-shifted with respect to the main transition of the monomeric [DAMS$^+$] NLO-phore as expected for a J-aggregation, while for the cofacial conformations such as A (eclipsed) and C ("head to tail" with $\alpha = 180°$) the blue-shifted transitions typical of H-type aggregation become significant. Notably, our calculated maximally responsive J-type configurations are considerably similar to the structures reported for [DAMS$^+$] PbI_3·2DMSO by Guloy et al.,[11] showing an interplanar distance close to 3.42 Å and a strongly slipped arrangement of the [DAMS$^+$] NLO-phores.

Starting from this body of observations and taking into account the good agreement between the experimental absorption spectrum of the [DAMS$^+$] monomer and that computed using B3LYP functional and 6-31g(d,p) basis set, we also computed the absorption spectra of the J-type aggregates corresponding to specific B_x and B_{xy} conformations at B3LYP/6-31g(d,p) level of theory. A detailed analysis of the TDDFT eigenvalues and eigenvectors for such specific B_x conformation shows, similar to the BP86/DZP results, a computed high-energy transition, III, at 2.77 eV ($f = 2.48$), which corresponds to intrachromophoric transitions, and two low-energy interchromophoric charge-transfer transitions, I and II, calculated at 1.88 eV ($f = 0.04$) and 2.18 eV ($f = 0.12$), see Table 3. The relative intensity of these three transitions strongly depends on their character because a large contribution from intrachromophoric transitions is related to a major intensity, as observed at the BP86/DZP level. Comparing the results obtained for the above transitions at B3LYP/6-31g(d,p) level to those obtained at BP86/DZP level, we observed an overall increase of bands associated with transitions I and II compared to that associated with transition III. The B3LYP/6-31g(d,p) computed values are in better agreement with the experimental values with respect to those computed at the BP86/DZP level; in particular, transition II at 2.18 eV (568 nm) can be related to the J-narrow band at 2.14 eV (580 nm), typical of the experimental absorption spectrum of J-aggregates of [DAMS$^+$].[15] The better agreement of the values calculated at the B3LYP level with respect to those calculated at the BP86 level can be originated by the Hatree−Fock exchange in the XC functional, which leads to an improved description of these partial charge-transfer transitions. For the B_{xy} conformation, a similar behavior is observed: the two low-energy transitions I and II are at higher energy (1.82 and 2.34 eV) compared to those calculated at the BP86/DZP level (1.21 and 1.86 eV), with increased oscillator strengths (see Table 3). However, the B_{xy} conformation provides a significant blue-shifted value of the energy of transition II compared to that of the B_x conformation and to the experimental value (2.34 vs 2.18 and 2.14 eV, respectively).

TABLE 4: Excitation Energies (eV), Oscillator Strengths, *f*, Dipole Moments, μ (D), and Transition Dipole Moments, *r* (D), Associated with the Ground States and Excited States Involved in Transitions I, II, and III for the Dimeric Configuration B_x with $d_z = 3.5$ and $d_x = 5.0$ Computed at the B3LYP/6-31g(d,p) Level[a]

	E	*f*	μ_x	μ_y	μ_z	μ_{tot}	r_x	r_y	r_z
S_0			11.2	−2.1	−0.3	11.4			
S_1	1.88	0.04	26.1	0.0	16.5	30.8	−0.82	0.06	−0.29
S_2	2.18	0.12	−17.5	−0.4	−15.7	23.8	1.44	−0.11	0.44
S_3	2.77	2.48	0.7	−0.2	−0.7	1.0	5.95	0.05	−0.79

[a] The dimer is oriented with the long molecular axis along the *x* axis, and the *z* axis corresponds to the interplanar distance.

Different from the known experimental absorption spectra of J-aggregates,[8,15] computed transition II, typical of J-aggregation, is always much less intense than the intrachromophoric transition III of monomeric [DAMS$^+$]. However, we have investigated only dimeric aggregates of [DAMS$^+$] units, whereas in the experimental spectra of crystalline materials J-aggregates of higher dimensions are involved, thus probably producing a higher intensity of the transition typical of J-aggregation. In summary, we have shown the interchromophoric origin of the typical absorption band of J-aggregates red-shifted with respect to the main intrachromophoric absorption band of the monomeric NLO-phore [DAMS$^+$] due to the splitting of HOMO and LUMO of specific arrangements of either B_x or B_{xy} conforma-

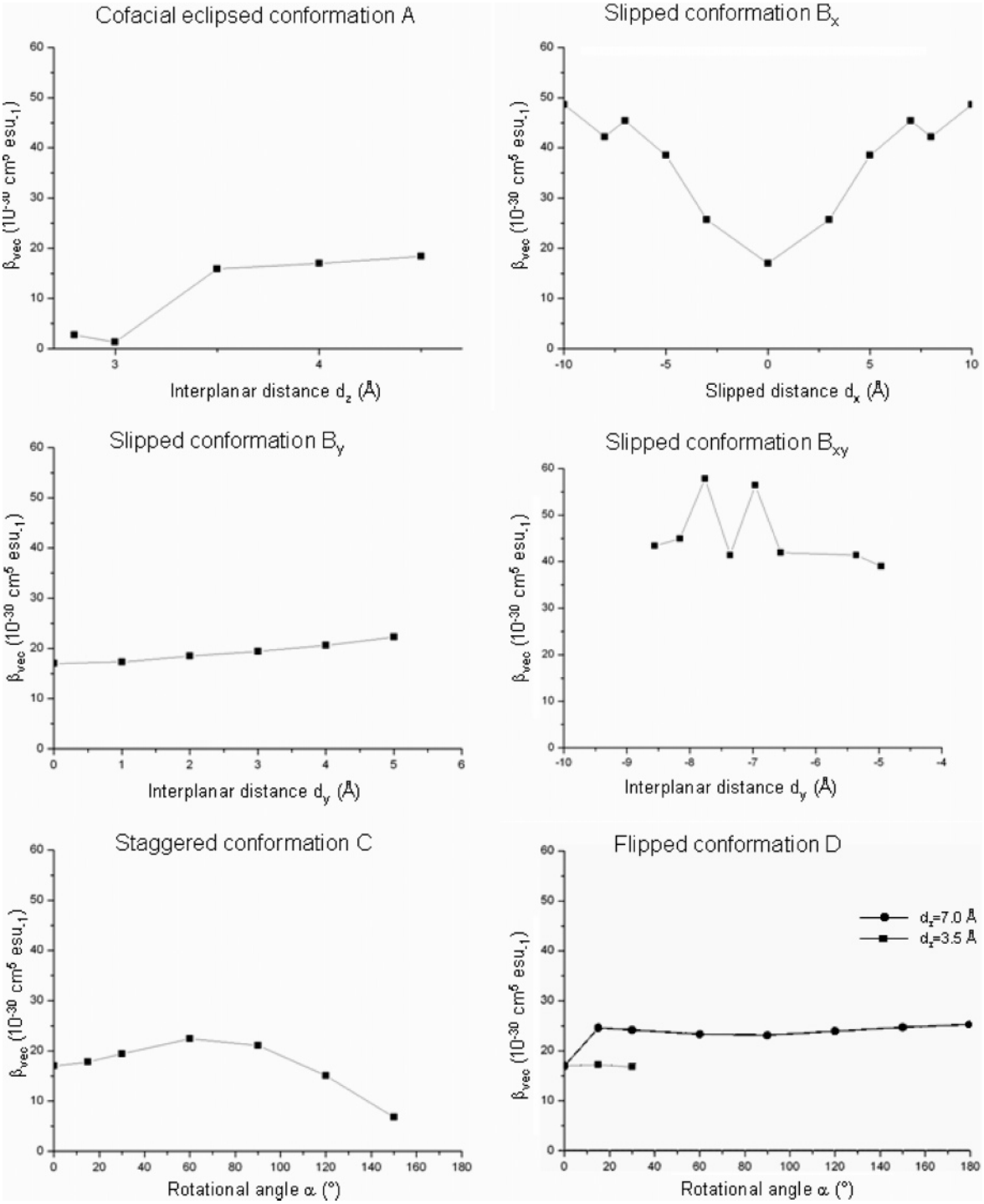

Figure 6. Calculated static β_{vec} values for A, B_x, B_{xy}, B_y, C, and D conformations as a function of d_x, d_y, and α ($d_z = 3.5$ Å).

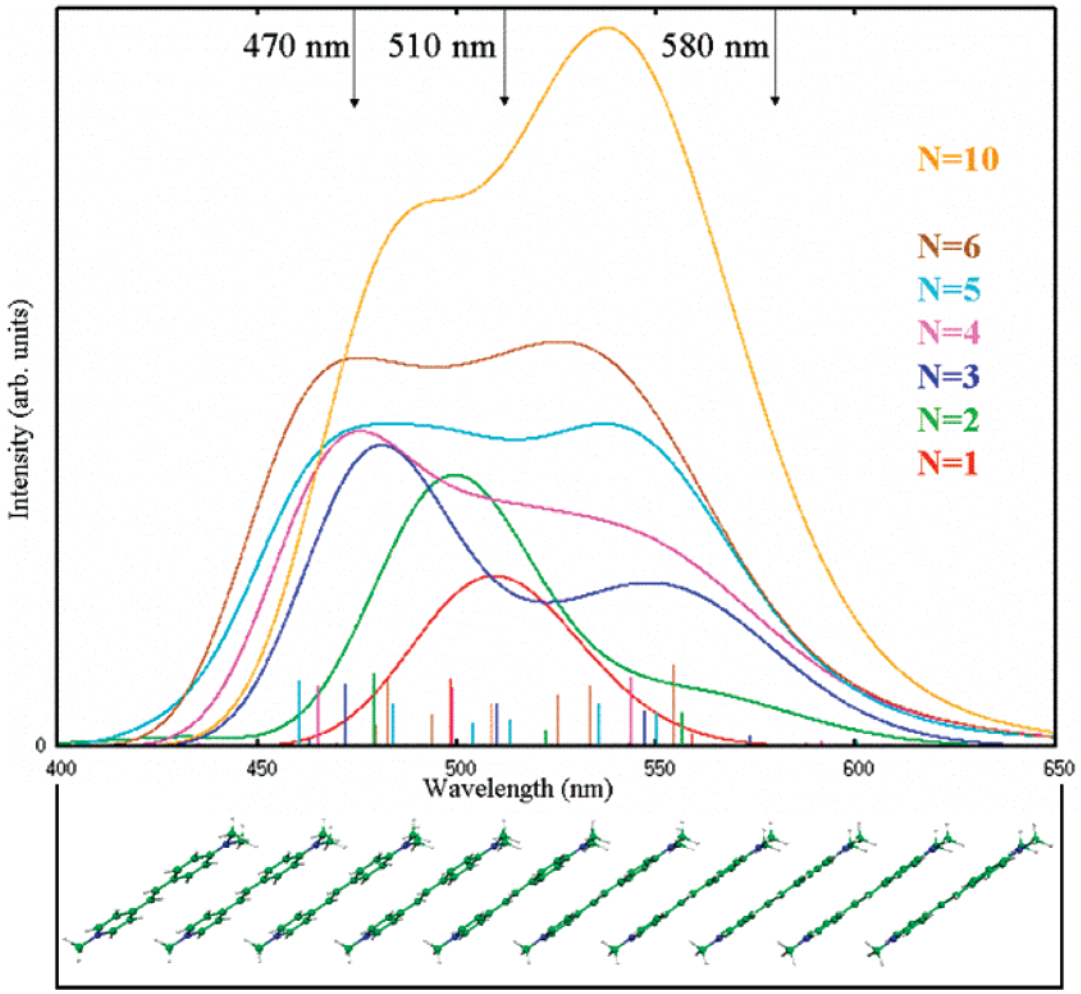

Figure 7. Calculated absorption spectra of the monomeric [DAMS$^+$] (red line) and of oligomers of increasing dimension up to 10 chromophore units. The arrows signal the experimental absorption maxima of the monomer in CH_3CN solution (470 nm) and of the [DAMS$^+$][Cu_5I_6] material in the solid state[15] (510 and 580 nm).

tion, structurally corresponding to J-aggregation. We thus computed at the B3LYP/6-31g(d,p) level of theory the dipole moments (Table 4) associated with the ground state and to the lowest singlet excited states S_1, S_2, and S_3 of transitions I, II, and III of the above B_x and B_{xy} dimeric conformations together with the associated oscillator strengths and transition dipole moments, giving in this way an estimate of the charge redistribution originated by these transitions. It is worth noting that the S_1 and S_2 excited states have very high dipole moments compared to those of the ground state and of S_3, in line with the nature of these excited states, mainly involving interchromophoric transitions. According to the approximate SOS approach discussed above, see Method and Computational Details, the low-energy transitions I and II typical of J-aggregates with their large variations of the ground- to excited-state dipole moments should provide a large contribution to the second-order NLO response, even considering their computed rather small oscillator strengths and transition dipole moments.

Figure 6 shows the calculated values of β_{vec} at the BP86/DZP level at zero frequency for the A, B_x, B_{xy}, B_y, C, and D conformations (for B_x, B_{xy}, B_y, and C, only calculations with $d_z = 3.5$ Å have been carried out); frequency-dependent β_{vec} values are reported as Supporting Information. For the eclipsed cofacial configuration A, corresponding to a H-type aggregation, a quenching of β_{vec} is observed by decreasing the interchromophoric distance d_z, as expected because the excited states that originated by interaction of the cofacial monomers are quenched by symmetry, while a significant drop of β_{vec} is calculated for d_z below 3.0 Å, due to strong overlap of the two parallel interacting NLO-phores. For the B_x conformation, calculated β_{vec} values show, as expected, a minimum in correspondence to the eclipsed cofacial arrangement, with increasing values by increasing the d_x slippage. This trend partially reflects the nature of the excited states involved, as discussed above, where the maximum calculated optical response occurs at $d_x = \pm 5.0$ Å, that is for J-aggregation. Interestingly, for the B_y, C, and D conformations calculated β_{vec} are almost insensitive to the relative position of the NLO-phores.

3.3. Theoretical Investigation of the Absorption Spectra of Oligomers of J-Type Aggregates of [DAMS$^+$]. Because in crystalline materials J-aggregates are arranged as oligomeric series within the crystal lattice,[9−15] to investigate beyond dimeric arrangements we performed semiempirical ZINDO calculations on a model corresponding to the B_x slipped conformation with $d_z = 3.5$ and $d_x = 5.0$ (J-aggregation) taking into accounts up to 10 units of the NLO-phore [DAMS$^+$]. The resulting absorption spectra calculated from $n = 1-10$ are reported in Figure 7. As can be noticed, the absorption spectrum of [DAMS$^+$] calculated at the semiempirical ZINDO level is slightly red-shifted compared to the experimental one (absorption maximum at 515 vs 471 nm) and to both BP86/DZP and B3LYP/6-31g(d,p) calculated values, 496 and 460 nm, respectively. Upon moving from the monomeric [DAMS$^+$] to the dimeric arrangement, an additional lower energy transition is calculated in line

with the TDDFT approach at the B3LYP/6-31g(d,p) level, as discussed above, although slightly more intense compared to that computed for the parent transition by TDDFT calculations. Even in the ZINDO approach the new red-shifted transition originates from interchromophoric charge-transfer excitations. Most notably, upon increasing the number of NLO-phore units, the lower-energy transition gains considerably intensity and for $n = 6$ the intrachromophoric and interchromophoric transitions have essentially the same intensity. For $n = 10$, the largest oligomer investigated, the interchromophoric transition becomes considerably more intense than the intrachromophoric one. Therefore, these ZINDO calculations reproduce the spectroscopic feature characteristic of J-type aggregation quite well because the calculated spectrum for $n = 10$, although slightly red-shifted compared to the experimental values (515 nm with respect to 471 nm), nicely reproduces the relative peak positions and in particular the relative intensities of the experimental absorption spectrum of J-aggregates.[9−15] Interestingly, our calculations predict the intrachromophoric band of the monomer [DAMS$^+$] to become less and less intense with respect to the red-shifted interchromophoric band, typical of J-aggregates, as the number of NLO-phores arranged as oligomers of J-aggregates increases, so that the relative intensity of the intrachromophoric and interchromophoric bands might be used to estimate the order of magnitude of "effectively" J-aggregated NLO-phores. We also evaluated the hyperpolarizability of monomer, dimer, and trimer aggregates by means of the approximate SOS approach. It is worth noting that, while the calculated hyperpolarizability of the dimer is twice the corresponding value of the monomer, for the trimer we calculated a NLO response 3.6 times larger than that of the monomer, thus confirming a cooperative effect on the increased second-order NLO response due to J-aggregation, starting from clusters with $n > 2$. Obviously, our simple oligomeric model does not reproduce the various kinds of oligomeric arrangements of J-aggregates of [DAMS$^+$] formed in crystalline materials, but it gives a qualitative view, in agreement with the experimental evidence, of the main features of the absorption spectra of this kind of materials.

4. Conclusions

Our DFT and TDDFT calculations on different dimeric aggregates of the NLO-phore [DAMS$^+$] have shown that J-aggregation, corresponding for instance to the dimeric parallel conformation B_x of [DAMS$^+$] with a reciprocal slippage along x of half molecule of 5.0 Å and an interchromophoric distance d_z of 3.5 Å, is associated with a splitting of HOMO and LUMO energy levels, characterized by the appearance of two new interchromophoric less intense transitions red-shifted with respect to the main intrachromophoric transition of monomeric [DAMS$^+$]. Therefore, the calculated absorption spectrum of this kind of conformation nicely reproduces the main feature typical of J-aggregation, corresponding to an additional absorption band red-shifted with respect to the main absorption band of monomeric [DAMS$^+$]. In particular, our TDDFT calculations on dimeric conformations and ZINDO calculations on oligomeric associations of [DAMS$^+$] have shown also that such a red-shifted band, associated with the new lower energy transitions, is of charge-transfer nature as expected for their interchromophoric origin. It follows that such new lower energy transitions are the origin of a significant cooperative additional effect on the second-order NLO response, stronger than that originated by the higher energy intramolecular transition of the monomeric [DAMS$^+$].

In crystalline materials, J-aggregation of NLO-phores such as [DAMS$^+$] appears to be organized as pseudo-oligomeric arrangements to produce a macropolarity along the crystalline network. Our ZINDO calculations, carried out on a simple model of oligomeric arrangements of J-type aggregates, have shown that oligomers with more than 5 or 6 [DAMS$^+$] units produce already a strong increase of the intensity of the red-shifted absorption bands associated with the above-mentioned interchromophoric transitions, which become stronger than the main absorption band associated with the major intramolecular transition of monomeric [DAMS$^+$]. This observation is in accordance with the spectroscopic features typical of crystalline hybrid materials with J-aggregates of [DAMS$^+$] in their crystal lattice.[9−15] Moreover, the calculated second-order NLO response associated with this new red-shifted absorption band leads, for the trimer, to a hyperpolarizability value 3.6 times larger than that of monomer. Therefore, our calculations have shown the nature and origin of significant cooperative contribution to the second-order NLO response, which is experimentally related to J-aggregation of molecular NLO-phores such as [DAMS$^+$].[6,9−15]

Finally, as a byproduct of our investigation centered on J-aggregation, we have shown that cofacial A or C conformations, corresponding to H-aggregation, give rise to a splitting of HOMO−LUMO energy levels as well, with generation of new transitions but at higher energy with respect to that of [DAMS$^+$]. These higher energy transitions are thus associated with new absorption bands blue-shifted with respect to the main intrachromophoric absorption band of monomeric [DAMS$^+$], a feature typical of the experimental spectra of H-aggregates.

In conclusion, our investigation has allowed us to gain considerable insight into the electronic structures responsible for the typical spectroscopic features of J- and H-aggregates of [DAMS$^+$] and also of the electronic origin, due to an interchromophoric charge-transfer process, of the significant contribution to the second-order NLO response of [DAMS$^+$] associated with its J-aggregation. Because we have shown that oligomers of J-aggregates of [DAMS$^+$], already in a simple model of oligomeric arrangement, produce a strong increase in the intensity of the red-shifted absorption band associated with the new charge-transfer processes originated by J-aggregation of [DAMS$^+$], it would be relevant to investigate, despite the obvious problem of the size of calculations, how such a strong increase of the intensity is associated with the macropolarity generated along the crystal lattice of hybrid materials containing J-aggregates of [DAMS$^+$] with a parallel very strong increase of the second-order NLO response.

Acknowledgment. This work was supported by the Ministero dell'Istruzione, dell'Università e della Ricerca (Programma di ricerca FIRB, year 2003, Research Title: Molecular compounds and hybrid nanostructured materials with resonant and nonresonant optical properties for photonic devices; PRIN 2005: Progettazione ed autoorganizzazione di architetture molecolari per nanomagneti e sistemi optoelettronici) and Fondazione CARIPLO (2005, Nuovi materiali con nanoorganizzazione di cromofori in sistemi Host−Guest o su scaffold inorganico per dispositivi fotoluminescenti o optoelettronici).

Supporting Information Available: Computed excitation energies, oscillator strengths, and composition of the lowest singlet excited states and static and SHG hyperpolarizability values for the dimer in the cofacial A, slipped B_x, B_{xy}, and B_y, and staggered C and D configurations. This material is available free of charge via the Internet at http://pubs.acs.org.

References and Notes

(1) (a) Verbiest, T.; Houbrechts, S.; Kauranen, M.; Clays, K.; Persoons, A. *J. Mater. Chem.* **1997**, *7*, 2175. (b) Dalton, L. R.; Steier, W. H.; Robinson, B. H.; Zhang, C.; Ren, A.; Garner, S.; Chen, A.; Londergan, T.; Irwin, L.; Carlson, B.; Fifield, L.; Phelan, G.; Kincaid, C.; Amend, J.; Jen, A. *J. Mater. Chem.* **1999**, *9*, 1905. (c) Molecular Nonlinear Optics: Materials, Phenomena and Devices; Zyss, J., Ed.; *Chem. Phys.* **1999**, *245* (special issue).

(2) (a) Meredith, G. R. In *Nonlinear Optical Properties of Organic and Polymeric Materials*; Williams, J. D., Ed.; ACS Symposium Series, American Chemical Society: Washington, DC, 1983; pp 27−56. (b) *Nonlinear Optical Properties of Organic Molecules and Crystals*; Chemla, D. S., Zyss, J., Eds.; Academic Press: Orlando, FL, 1987; Vol. 1. (c) *Materials for Nonlinear Optics Chemical Perspectives*; Marder, S. R., Stucky, G. D., Sohn, J. E., Eds.; ACS Symposium Series 455; American Chemical Society: Washington, DC, 1991. (d) *Introduction to Nonlinear Optical Effects in Molecules and Polymers*; Prasad, P. N., Williams, D. J., Eds.; John Wiley: New York, 1991. (e) *Molecular Nonlinear Optics: Materials, Physics and Devices*; Zyss, J., Ed.; Academic Press: New York, 1994. (f) *Organic Nonlinear Optical Materials*; Bosshard, C., Sutter, K., Prêtre, P., Hulliger, J., Flörsheimer, M., Kaatz, P., Günter, P., Eds.; Advances in Nonlinear Optics; Gordon & Breach: Amsterdam, 1995; Vol. 1. (g) *Nonlinear Optics of Organic Molecules and Polymers*; Nalwa, H. S., Miyata, S., Eds.; CRC Press: Boca Raton, FL, 1997. (h) *Characterization Techniques and Tabulations for organic Nonlinear Optical Materials*; Kuzyk, M. G., Dirk, C. W., Eds.; Marcel Dekker: New York, 1998.

(3) Marks, T. J.; Ratner, M. A. *Angew. Chem., Int. Ed. Engl.* **1995**, *34*, 155.

(4) (a) Jen, A. K.-Y.; Cai, Y. M.; Bedworth, P. V.; Marder, S. R. *Adv. Mater.* **1997**, *9*, 132. (b) Ma, H.; Jen, A. K.-Y.; Dalton, L. R. *Adv. Mater.* **2002**, *14*, 1339.

(5) Marder, S. R.; Perry, J. W.; Yakymyshyn, C. P. *Chem. Mater.* **1994**, *6*, 1137.

(6) Lacroix, P. G.; Clément, R.; Nakatani, K.; Zyss, J.; Ledoux, I. *Science* **1994**, *263*, 658.

(7) Möbius, D. *Adv. Mater.* **1995**, *7*, 437.

(8) Whitten, D. G. *Acc. Chem. Res.* **1993**, *26*, 502.

(9) Corradin, T.; Clément, R.; Lacroix, P. G.; Nakatani, K. *Chem. Mater.* **1996**, *8*, 2153.

(10) Bénard, S.; Yu, P.; Audière, J. P.; Rivière, E.; Clément, R.; Guilhem., J.; Tchertanov, L.; Nakatani, K. *J. Am. Chem. Soc.* **2000**, *122*, 9444.

(11) Guloy, A. M.; Tang, Z.; Miranda, P. B.; Srdanov, V. I. *Adv. Mater.* **2001**, *13*, 833.

(12) Yi, T.; Tancrez, N.; Clément, R.; Ledoux-Rak, I.; Zyss, J. *J. Lumin.* **2004**, *110*, 389.

(13) Yi, T.; Clément, R.; Haut, C.; Catala, L.; Gacoin, T.; Tancrez, N.; Ledoux, I.; Zyss, J. *Adv. Mater.* **2005**, *17*, 335.

(14) Clément, R.; Lacroix, P. G.; O'Hare, D.; Evans, J. *Adv. Mater.* **1994**, *6*, 794.

(15) (a) Cariati, E.; Ugo, R.; Cariati, F.; Roberto, D.; Masciocchi, N.; Galli, S.; Sironi, A. *Adv. Mater.* **2001**, *13*, 1665. (b) Cariati, E.; Pizzotti, M.; Roberto, D.; Tessore, F.; Ugo, R. *Coord. Chem. Rev.* **2006**, *250*, 1210.

(16) (a) Di Bella, S.; Ratner, M. A.; Marks, T. J. *J. Am. Chem. Soc.* **1992**, *114*, 5842. (b) Di Bella, S.; Fragalà, I.; Ratner, M. A.; Marks, T. J. *J. Am. Chem. Soc.* **1993**, *115*, 682. (c) Kanis, D. R.; Ratner, M. A.; Marks, T. J. *Chem. Rev.* **1994**, *94*, 195. (d) Di Bella, S.; Fragalà, I.; Ratner, M. A.; Marks, T. J. *Chem. Mater.* **1995**, *7*, 400. (e) Di Bella, S.; Lanza, G.; Fragalà, I.; Yitzchaik, S.; Ratner, M. A.; Marks, T. J. *J. Am. Chem. Soc.* **1997**, *119*, 3003. (f) Yitzchaik, S.; Di Bella, S.; Lundquist, P. M.; Wong, G. K.; Marks, T. J. *J. Am. Chem. Soc.* **1997**, *119*, 2995.

(17) Cornil, J.; dos Santos, D. A.; Crispin, X.; Silbey, R.; Brédas, J. L. *J. Am. Chem. Soc.* **1998**, *120*, 1289.

(18) Gonbeau, D.; Coradin, T.; Clément, R. *J. Phys. Chem. B* **1999**, *103*, 3545.

(19) Apitz, D.; Bertram, R. P.; Benter, N.; Hieringer, W.; Andreasen, J. W.; Nielsen, M. N.; Johansen, P. M.; Buse, K. *Phys. Rev. E* **2005**, *72*, 036610.

(20) (a) Ray, P. C.; Leszczynski, J. *Chem. Phys. Lett.* **2006**, *419*, 578. (b) Ray, P. C.; Bonifassi, P.; Leszczynski, J. *J. Phys. Chem. A* **2006**, *110*, 8963.

(21) Kanis, D. R.; Lacroix, P. G.; Ratner, M. A.; Marks, T. J. *J. Am. Chem. Soc.* **1994**, *116*, 10089.

(22) Barlow, S.; Bunting, H. E.; Ringham, C.; Green, J. C.; Bublitz, G. U.; Boxer, S. G.; Perry, J. W.; Marder, S. R. *J. Am. Chem. Soc.* **1999**, *121*, 3715.

(23) Hieringer, W.; Baerends, E. J. *J. Phys. Chem. A* **2006**, *110*, 1014.

(24) Champagne, B.; Perpète, E. A.; Jaquemin, D.; van Gisbergen, S. J. A.; Baerends, E. J.; Soubra-Ghaoui, C.; Robins, K. A.; Kirtman, B. *J. Phys. Chem. A* **2000**, *104*, 4755.

(25) (a) Fournier, R.; Andzelm, J.; Salahub, D. R. *J. Chem. Phys.* **1989**, *90*, 6371. (b) Komornicki, A.; Fitzgerald, G. *J. Chem. Phys.* **1993**, *98*, 1398.

(26) (a) Casida, M. E. *Time-Dependent Density Functional Response Theory for Molecules*; Chong, D. P., Ed.; World Scientific: Singapore, 1995; Vol. 1, pp 155−192. (b) van Gisbergen, S. J. A.; Snijders, J. G.; Baerends, E. J. *J. Chem. Phys.* **1998**, *109*, 10644.

(27) Orr, B. J.; Ward, J. F. *Mol. Phys.* **1971**, *20*, 513.

(28) Oudar, J. L.; Chemla, D. S. *J. Phys. Chem.* **1977**, *66*, 2664.

(29) (a) Fantacci, S.; De Angelis, F.; Selloni, A. *J. Am. Chem. Soc.* **2003**, *125*, 4381. (b) De Angelis, F.; Fantacci, S.; Selloni, A. *Chem. Phys. Lett.* **2004**, *389*, 204. (c) Fantacci, S.; De Angelis, F.; Sgamellotti, A.; Re, N. *Chem. Phys. Lett.* **2004**, *396*, 43. (d) Fantacci, S.; De Angelis, F.; Wang, J.; Bernhard, S.; Selloni, A. *J. Am. Chem. Soc.* **2004**, *126*, 8718. (e) Fantacci, S.; De Angelis, F.; Sgamellotti, A.; Marrone, A.; Re, N. *J. Am. Chem. Soc.* **2005**, *127*, 14144.

(30) Tozer, D. J.; Amos, R. D.; Handy, N. C.; Roos, B. O.; Serrano-Andres, L. *Mol. Phys.* **1999**, *97*, 859−868.

(31) (a) Dreuw, A.; Weisman, J. L.; Head-Gordon, M. *J. Chem. Phys.* **2006**, *119*, 557. (b) Dreuw, A.; Fleming, G. R.; Head-Gordon, M. *J. Phys. Chem. B* **2003**, *107*, 6500. (c) Dreuw, A.; Head-Gordon, M. *J. Am. Chem. Soc.* **2004**, *126*, 4007. (d) Dreuw, A.; Head-Gordon, M. *Chem. Phys. Lett.* **2006**, *426*, 231.

(32) (a) Hieringer, W.; Görling, A. *Chem. Phys. Lett.* **2006**, *419*, 557. (b) Hieringer, W.; Görling, A. *Chem. Phys. Lett.* **2006**, *426*, 234.

(33) Frisch, M. J.; Trucks, G. W.; Schlegel, H. B.; Scuseria, G. E.; Robb, M. A.; Cheeseman, J. R.; Montgomery, J. A., Jr.; Vreven, T.; Kudin, K. N.; Burant, J. C.; Millam, J. M.; Iyengar, S. S.; Tomasi, J.; Barone, V.; Mennucci, B.; Cossi, M.; Scalmani, G.; Rega, N.; Petersson, G. A.; Nakatsuji, H.; Hada, M.; Ehara, M.; Toyota, K.; Fukuda, R.; Hasegawa, J.; Ishida, M.; Nakajima, T.; Honda, Y.; Kitao, O.; Nakai, H.; Klene, M.; Li, X.; Knox, J. E.; Hratchian, H. P.; Cross, J. B.; Bakken, V.; Adamo, C.; Jaramillo, J.; Gomperts, R.; Stratmann, R. E.; Yazyev, O.; Austin, A. J.; Cammi, R.; Pomelli, C.; Ochterski, J. W.; Ayala, P. Y.; Morokuma, K.; Voth, G. A.; Salvador, P.; Dannenberg, J. J.; Zakrzewski, V. G.; Dapprich, S.; Daniels, A. D.; Strain, M. C.; Farkas, O.; Malick, D. K.; Rabuck, A. D.; Raghavachari, K.; Foresman, J. B.; Ortiz, J. V.; Cui, Q.; Baboul, A. G.; Clifford, S.; Cioslowski, J.; Stefanov, B. B.; Liu, G.; Liashenko, A.; Piskorz, P.; Komaromi, I.; Martin, R. L.; Fox, D. J.; Keith, T.; Al-Laham, M. A.; Peng, C. Y.; Nanayakkara, A.; Challacombe, M.; Gill, P. M. W.; Johnson, B.; Chen, W.; Wong, M. W.; Gonzalez, C.; Pople, J. A. *Gaussian 03*, revision C.02; Gaussian, Inc.: Wallingford, CT, 2004.

(34) van Gisbergen, S. J. A.; Snijders, J. G.; Baerends, E. J. *Comput. Phys. Chem.* **1999**, *118*, 119.

(35) te Velde, G.; Bickelhaupt, F. M.; Baerends, E. J.; Fonseca-Guerra, C.; van Gisbergen, S. J. A.; Snijders, J. G.; Ziegler, T. *J. Comput. Chem.* **2001**, *22*, 931.

(36) (a) Ridley, J. E.; Zerner, M. C. *Theor. Chim. Acta* **1973**, *32*, 111. (b) Ridley, J. E.; Zerner, M. C. *Theor. Chim. Acta* **1976**, *42*, 223. (c) Bacon, A. D.; Zerner, M. C. *Theor. Chim. Acta* **1979**, *53*, 21. (d) Zerner, M. C.; Lowe, G. H.; Kirchner, R. F.; Mueller,-Westerhoff, U. T. *J. Am. Chem. Soc.* **1980**, *102*, 589. (e) Zerner, M. C.; Correa de Mello, P.; Hehenberger, M. *Int. J. Quantum Chem.* **1982**, *21*, 251. (f) Anderson, W. P.; Esdwards, W. D.; Zerner, M. C. *Inorg. Chem.* **1986**, *25*, 2728. (g) Hanson, L. K.; Fajer, J.; Thompson, M. A.; Zerner, M. C. *J. Am. Chem. Soc.* **1987**, *109*, 4728. (h) Thompson, M. A.; Zerner, M. C. *J. Am. Chem. Soc.* **1991**, *113*, 8210. (i) Zerner, M. C. In *Reviews in Computational Chemistry*; Lipkowitz, K. B., Boyd, D. B., Eds.; VCH Publishing: New York, 1991; Vol. 2, p 313.

(37) Becke, A. D. *Phys. Rev. A* **1988**, *38*, 3089.

(38) Perdew, J. P. *Phys. Rev. B* **1986**, *33*, 8822.

(39) Vosko, S. H.; Wilk, L.; Nusair, M. *Can. J. Phys.* **1980**, *58*, 1200.

(40) van Leeuwen, R.; Baerends, E. J. *Phys. Rev. A* **1994**, *49*, 2421.

(41) Becke, A. D. *J. Chem. Phys.* **1993**, *98*, 5648−5652.

(42) Ditchfield, R.; Hehre, W. J.; Pople, J. A. *J. Chem. Phys.* **1971**, *54*, 724−728.

(43) (a) Barone, V.; Cossi, M. *J. Phys Chem. A* **1998**, *102*, 1995−2001. (b) Cossi, M.; Rega, N.; Scalmani, G.; Barone, V. *J. Comput. Chem.* **2003**, *24*, 669−681. (c) Cossi, M.; Barone, V. *J. Chem. Phys.* **2001**, *115*, 4708−4717.

(44) Willetts, A.; Rice, J. E.; Burland, D. M.; Shelton, D. P. *J. Chem. Phys.* **1992**, *97*, 7590.

(45) Wiberg, K. B.; Hadad, C. M.; LePage, T. J.; Breneman, C. M.; Frisch, M. *J. Phys. Chem.* **1992**, *96*, 671.

(46) *HyperCube HYPERCHEM*, Release 8 for Windows, HyperCube.

(47) Cambridge Crystallographic Data Centre, November 2005.

(48) Ogawa, K.; Takashi, S.; Yoshimura, S.; Takeuchi, Y.; Toriumi, K. *J. Am. Chem. Soc.* **1992**, *114*, 1041.

(49) Bruni, S.; Cariati, E.; Cariati, F.; Manassero, L.; Barcolli, W.; Roberto, D.; Ugo, R. In *Syntheses and Methodologies in Inorganic Chemistry*; Daolio, S., Fabrizio, M., Tondello, E., Armelao, L., Vigato, P. A., Eds.; Albignasego: Padova, 2000; pp 162−5 and Ugo et al. to be published.

(50) Characterization of the nature of the TDDFT transitions in terms of single orbital excitations is usually possible, provided one has access to

the eigenvectors. The latter are made up of two component vectors, X and Y, related to single-particle excitations and de-excitations, respectively. In G03, however, the program only provides the (dominant) components of the sum vector X + Y, and it is thus impossible in principle to separate the interfering excitation and de-excitation components. To the extent, however, that we may reasonably assume that the de-excitation vector Y is small compared to X (it would be exactly zero in the Tamm−Dancoff or single excitation CI approximation), we may take the square of the X + Y vector components as a qualitative measure of the weight pertaining to the corresponding single excitations. For closed-shell molecules, the G03 TDDFT vectors are actually normalized to $^1/_2$ (with the normalization condition $<X - Y|X + Y> = {}^1/_2$), so we take the double of the squared coefficients. The results thus obtained for our calculations are those displayed in Table 3.